Journal of Non-Crystalline Solids 357 (2011) 2604–2610

Contents lists available at ScienceDirect

Journal of Non-Crystalline Solids

journal homepage: www.elsevier.com/ locate/ jnoncrysol

# Interpretation of the Ni K-edge EXAFS in nanocrystalline nickel oxide using molecular dynamics simulations

A. Anspoks, A. Kuzmin *

*Institute of Solid State Physics, University of Latvia, Kengaraga street 8, LV-1063 Riga, Latvia*

ARTICLE INFO

*Article history:*
Received 17 September 2010
Received in revised form 14 February 2011
Available online 9 March 2011

*Keywords:*
NiO;
Ni K-edge;
EXAFS;
Molecular dynamics;
Nanoparticles

ABSTRACT

Analysis of atomic structure at the nanoscale is a challenging task, complicated by relaxation phenomena and thermal disorder. In this work, the x-ray absorption spectroscopy at the Ni K-edge was used to address this problem in nanocrystalline NiO (nano-NiO) at 300 K. The analysis of the first two coordination shells using conventional two-shell single-scattering approximation allowed us to determine the expansion of the average lattice but contraction of the Ni—O bonds in the first coordination shell in nano-NiO in comparison with the bulk nickel oxide. The EXAFS signal generated within the first six coordination shells (up to ~6.5 Å) was successfully interpreted using classical molecular dynamics and ab initio multiple-scattering EXAFS theory. We found that simple rigid-ion force-field model is able to describe the structure relaxation and dynamics in both bulk and nano-NiO. Such approach requires less parameters than conventional EXAFS analysis and allows accounting explicitly for thermal effects and many-atom distribution functions. Finally, we showed that the EXAFS signal is rather sensitive to small variations of the force-field model and, thus, the agreement between the experimental and calculated EXAFS signals can be used for the force-field model optimization.


## 1. Introduction

Determination of atomic structure at the nanoscale is far from trivial task, complicated additionally by atomic structure relaxation. The problem can be addressed within a complex modeling approach combining the experimental results and the theory in some effective way [1]. Among different experimental techniques applicable to nanostructured materials, only scattering/diffraction methods and x-ray absorption spectroscopy (EXAFS) provide with the direct structural information. The former methods, gaining popularity for nanostructure studies under the name of the total scattering/PDF analysis [2], contain information on the atomic pair distribution functions (PDFs).

At the same time, the EXAFS spectra include also contributions from many-atom distribution functions, which, however, are difficult to access [3]. The current EXAFS theory implementation allows treating this problem within one of two schemes. The most popular approach relies on a distribution of instantaneous interatomic distances contributing into the multiple-scattering paths [3], whereas another one uses a configurational averages of the EXAFS signals over *n*-atom distributions [4–6]. In both cases, the knowledge (or a guess) of the average atomic structure and the treatment of thermal disorder are required. The latter is conventionally addressed using phenomenological models, such as the correlated Einstein and Debye models, Gaussian or cumulant approximations [3]. However, in a situation, when there are many structurally different atomic sites, a configuration averaged EXAFS signal can be generated more accurately from a set of atomic configurations, obtained from Monte Carlo (MC) [7], Molecular Dynamics (MD) [8–15], or Reverse Monte Carlo (RMC) [16–18] simulations. The use of these advanced approaches to extract the three-dimensional nanoparticle structure from the total EXAFS signal is a challenging task.

Chemical and physical properties of nanoparticles are directly connected to their shape and size [19]. The reduction in size causes usually the atomic structure relaxation, leading to compression or expansion of the average unit cell volume. While the volume compression is common for metal nanoparticles, its expansion is observed in most nano-metal-oxides [20–24]. In particular, the lattice expansion has been found recently by x-ray diffraction [25,26] in nanocrystalline NiO, having a size below about 30 nm.

The structure of NiO nanoparticles and thin films has been also studied in the past by Ni K-edge EXAFS using multi-shell single-scattering and multiple-scattering approaches [27–29].

The structure of the $NiO_x$ thin films, produced by reactive dc magnetron sputtering, has been described within the non-reconstructed grain-boundary model with the average crystallites size in the range of 2.1–3.4 nm [27]. The small size of crystallites resulted in a reduction of the nickel coordination number and an increase of the structural disorder by $\Delta\sigma^2 \approx 0.003–0.009$ Å$^2$ and the lattice parameter by $\Delta a \approx 0.016–0.034$ Å, compared to bulk nickel oxide (c-NiO) [27].

An increase of disorder at the superficial sites without evidence of a significant reduction of coordination numbers due to the size of the

* Corresponding author.
*E-mail address:* a.kuzmin@cfi.lu.lv (A. Kuzmin).
*URL:* http://www.cfi.lv (A. Kuzmin).

0022-3093/$ – see front matter © 2011 Elsevier B.V. All rights reserved.
doi:10.1016/j.jnoncrysol.2011.02.030

NiO crystallites has been found in the NiO–$SiO_2$ nanocomposites produced by sol-gel technology and containing NiO nanoparticles with an average dimension of 10 nm [28]. Polarization-dependent EXAFS study of 3 and 10 monolayer (ML) thick NiO film, grown on Ag (001), has evidenced the presence of the in-plane and out-of-plane strains in the film, but no disorder amount has been reported [29].

One should point out that in both works [28] and [29] several constrains have been used in the EXAFS model to reduce the number of fitting parameters and a correlation between the coordination numbers $N$ and the Debye–Waller (DW) factors $\sigma^2$. In [28] the coordination numbers were fixed to the values for bulk c-NiO, whereas the values of interatomic distances and the DW factors were free to vary. The variation of distances was additionally constrained in [29] by a single parameter, representing the isotropic volume change (expansion or contraction). While such approach is commonly used and helps to stabilize a solution during the fit, a large number of independent (or connected via simplified relationships) fitting parameters in the presence of many multiple-scattering paths makes the obtained numerical values, primarily for the DW factors, unreliable even when the good fit is achieved. The problem becomes more serious in the case of large non-Gaussian disorder or in compounds with strong multiple-scattering contributions generated within near-linear atomic chains as in rock-salt-type NiO. In the latter case, the atoms vibrations perpendicular to the linear atomic chain will significantly influence the EXAFS signal amplitude due to the strong angular dependence of the focussing effect [30].

In this work we present the results of the Ni K-edge EXAFS interpretation in crystalline and nanocrystalline NiO, obtained by joined use of classical molecular dynamics (MD) and ab initio multiple-scattering EXAFS theory [31]. The use of MD allows to constrain a structural solution by introducing just a few force field model parameters and to gain an access to both structure and dynamics of nickel oxide. A set of atomic configurations, generated from the MD run at desired experimental conditions, is further used to obtain configuration averaged EXAFS signal, whose agreement with the experimental data is finally used as a proof of the MD model reliability.

## 2. Experimental and data analysis

Black NiO nanoparticles (nano-NiO) were produced using a reaction of aqueous solutions of $Ni(NO_3)_2 \cdot 6H_2O$ salt and NaOH with subsequent annealing in air at 300 °C. The average size of nanoparticles was 13 nm according to the BET specific surface area measurements [37]. The nanocrystallites size of $6.2 \pm 1.8$ nm was estimated from the line broadening of the X-ray diffraction (111), (200), and (220) peaks, corrected for instrumental broadening, using the Scherrer's method and assuming the cubic crystallites shape. The commercial green polycrystalline nickel oxide (c-NiO, Aldrich, 99%) was used for comparison.

The Ni K-edge EXAFS signals were measured in transmission mode at the HASYLAB DESY C1 bending-magnet beamline at 300 K. The storage ring DORIS III operated at $E = 4.44$ GeV and $I_{max} = 140$ mA in a five bunches mode with a lifetime of 4 h. The higher-order harmonics were effectively eliminated by detuning of the monochromator Si (111) crystals to 60% of the rocking curve maximum, using the beam-stabilization feedback control. The x-ray beam intensity was measured by two ionization chambers filled with argon and krypton gases. The powder samples for x-ray absorption measurements were deposited on Millipore filters to give an absorption edge jump $\Delta\mu x \simeq 1$.

The x-ray absorption spectra were analyzed using the "EDA" software package [32]. The x-ray absorption near-edge structure (XANES) and the extended x-ray absorption fine structure (EXAFS) were extracted following conventional procedure [33] (Figs. 1 and 2). The EXAFS signals were modeled using two methods: (i) conventional multi-component approach within the single-scattering approxima-

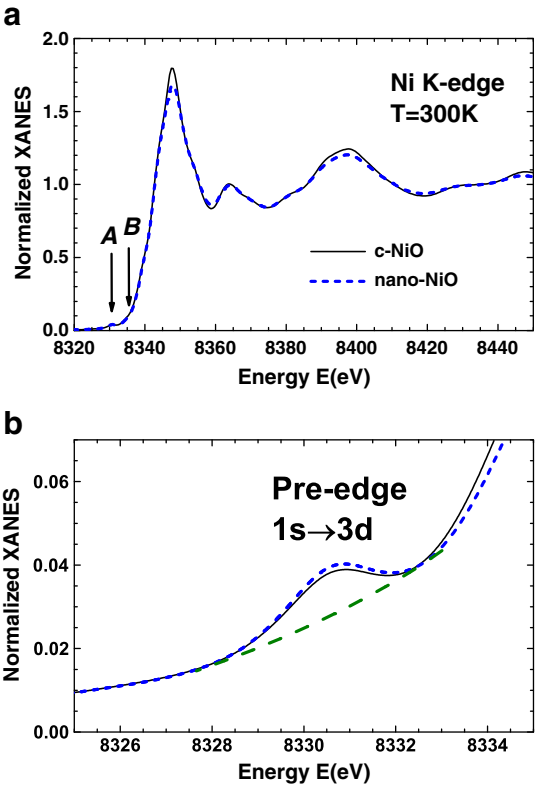


**Fig. 1.** Upper panel: Experimental Ni K-edge XANES in c-NiO (solid lines) and nano-NiO (dashed lines) at 300 K. The position of the pre-edge peak *A* and the next feature *B* are indicated by arrows. Lower panel: enlarged region of the pre-edge peak *A*.

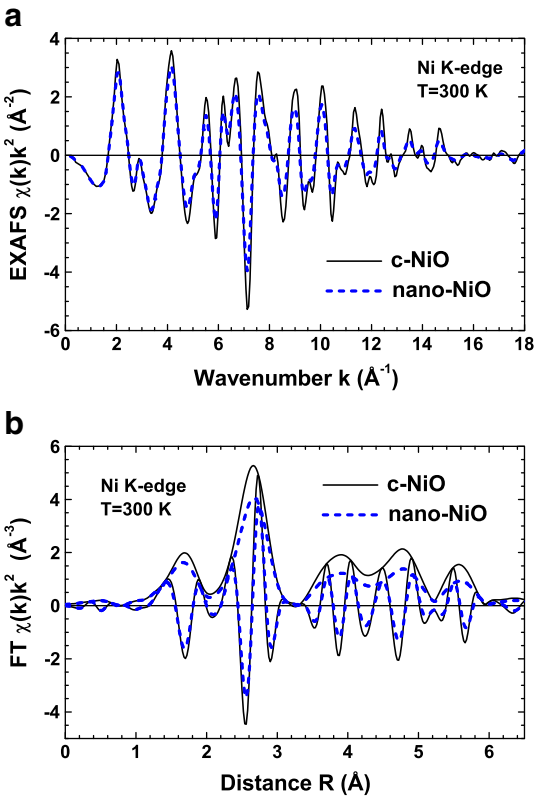


**Fig. 2.** Experimental Ni K-edge EXAFS $\chi(k)k^2$ signals and their Fourier transforms for c-NiO (solid lines) and nano-NiO (dashed lines) at 300 K.

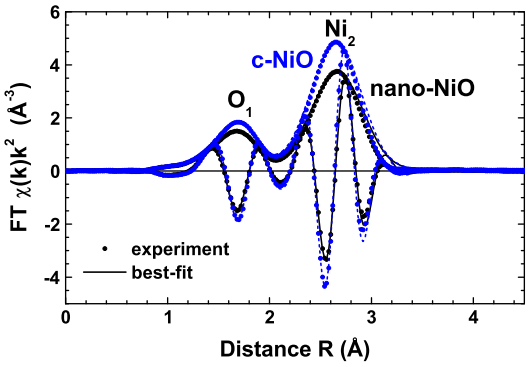


**Fig. 3.** Fourier transforms of the experimental (open circles) and calculated (solid lines) Ni K-edge EXAFS $\chi(k)k^2$ signals for c-NiO and nano-NiO within the range of the first two ($O_1$, $Ni_2$) coordination shells.

tion [33], and (ii) recently developed MD-EXAFS approach, based on the use of classical molecular dynamics (MD) and ab initio multiple-scattering theory [3].

In the conventional analysis, the contribution to the total EXAFS signal from the first two coordination shells (Ni–$O_1$ and Ni–$Ni_2$) was first isolated by the Fourier filtering procedure in the *R*-space range of 0.7–3.2 Å. Next, the two-component Gaussian model within the single-scattering approximation was used to best-fit the obtained EXAFS signal in the *k*-space range of 2–15 $Å^{-1}$. To perform EXAFS calculations, one requires the knowledge of the scattering amplitude and phase shift functions for the Ni—O and Ni—Ni atom pairs. Here they were calculated by the ab initio FEFF8 code [34]. The calculations were performed for the cluster of 8 Å size centered at absorbing nickel atom and having the cubic NiO structure [35]. The inelastic losses were taken into account using the complex exchange-correlation Hedin–Lundqvist potential [3]. The results of the best-fits are shown in Fig. 3. The obtained structural parameters, such as the coordination numbers (*N*), the interatomic distances (*R*) and the mean-squared relative displacements (MSRDs), known also as EXAFS Debye–Waller factors, ($\sigma^2$), are reported in Table 1.

## 3. MD-EXAFS simulations

To overcome the limitations of the conventional EXAFS analysis, we employed the method [3], based on the calculation of the configuration-averaged EXAFS signal using atomic configurations generated within classical molecular dynamics (MD) simulation. Note that the method enormously reduces the number of free model parameters to that required by the force-field description [3,36,38]. Besides, the method allows, in principle, to eliminate the use of the Fourier filtering procedure commonly employed in the conventional EXAFS data analysis, however this requires that the MD simulation box should be large enough to properly account for all coordination shells contributing into the experimental EXAFS signal. Finally, a refinement of the interatomic potentials based on the EXAFS spectra, i.e. the solution of the inverse problem, can be also performed, however this task, being very heavy computationally, is not addressed in the present work.

Here we performed first classical MD simulations in the canonical ensemble (NVT) by the GULP3.1 code [39], which is suitable for both crystalline and nanosized materials. Crystalline c-NiO was modeled by the supercell $6a_0 \times 6a_0 \times 6a_0$, where the lattice parameter $a_0 = 4.1773$ Å [35], with 3D periodic boundary conditions. The simulations for c-NiO were also performed for rhombohedrally distorted ($R\,3m$ space group) lattice to check the effect of weak magnetostriction distortion present in the antiferromagnetic phase below 523 K [40,41] on the EXAFS signal: it was found to be negligible.

The nanosized NiO was simulated by a cluster having the cubic shape and the size of up to $6a_0 \times 6a_0 \times 6a_0$. No boundary conditions were employed in this case. Our estimate for the cubic shape particles indicate that the EXAFS signal should feel the difference between crystal and nanoparticle when the particle size becomes smaller than about 400 Å. For larger particles, the contribution from atoms, located close to the surface and having reduced coordination, is too small to be detectable. Currently, the size of about 25 Å is the largest accessible technically to our simulations.

The force-field (FF) potential model, based on the two-body central force interactions, was employed in the MD simulations. It consists of a sum of the Buckingham and Coulomb potentials [39]

$$U_{ij}\left(r_{ij}\right) = A_{ij}exp\left(-r_{ij}/\rho_{ij}\right) - \frac{C_{ij}}{r_{ij}^6} + \frac{Z_i Z_j e^2}{r_{ij}}. \quad (1)$$

The Buckingham potential parameters (*A*, $\rho$, and *C* in Table 2) were taken from available data [42,43] for c-NiO. The formal ion charges *Z* ($Z = +2$ for Ni and $Z = -2$ for O) were used in the Coulomb potential [42,43]. We found that the Fisher's FF model [42] gives slightly better agreement with the experimental Ni K-edge EXAFS signal for c-NiO than the Oliver's one [43], therefore only the former was used in the simulation of nano-NiO. However, the original values of the Buckingham potential parameter $\rho$ in the Fisher's FF model [42] were manually adjusted (Table 2) for nano-NiO to reflect the change in the frequency of the experimental EXAFS signal being related to the lattice expansion (Table 1).

The Newton's equations were integrated by the leapfrog Verlet method [39]. In each simulation, the structure was first equilibrated during 20 ps at 300 K, corresponding to the temperature of the EXAFS experiments, and a set of instantaneous atomic configurations was accumulated during the 20 ps production run with a time step of 0.5 fs. Thus obtained sets of instantaneous atomic configurations were used to calculate the total radial distribution functions (RDFs) (Fig. 4), which were used to evaluate the values of MSRDs for the first and second shells.

Finally, the Ni K-edge EXAFS signals were calculated for each instantaneous atomic configuration using ab initio FEFF8 code [34].

**Table 1**
Structural parameters for the first and second coordination shells in c-NiO and nano-NiO obtained from the best-fit of the Ni K-edge EXAFS signals.

| | 1 shell (Ni—$O_1$) | 2 shell (Ni—$Ni_2$) |
|---|---|---|
| *c-NiO* | | |
| *N* | 6 ± 0.2 | 12 ± 0.4 |
| *R* (Å) | 2.070 ± 0.003 | 2.949 ± 0.003 |
| $\sigma^2$ ($Å^2$) | 0.0057 ± 0.0005 | 0.0067 ± 0.0005 |
| *nano-NiO* | | |
| *N* | 5.8 ± 0.2 | 11.3 ± 0.4 |
| *R* (Å) | 2.061 ± 0.003 | 2.961 ± 0.003 |
| $\sigma^2$ ($Å^2$) | 0.0077 ± 0.0005 | 0.0082 ± 0.0005 |

**Table 2**
Force field (FF) parameters of the Buckingham potentials for c-NiO and nano-NiO.

| Pair of atoms | *A* (eV) | $\rho$ (Å) | *C* (eV $Å^6$) |
|---|---|---|---|
| c-NiO | Oliver's FF [43] | | |
| $Ni^{+2}$—$O^{-2}$ | 775.0 | 0.3250 | 0.0 |
| $O^{-2}$—$O^{-2}$ | 22764.3 | 0.1490 | 20.37 |
| c-NiO | Fisher's FF [42] | | |
| $Ni^{+2}$—$O^{-2}$ | 754.92 | 0.3277 | 0.0 |
| $O^{-2}$—$O^{-2}$ | 22764.3 | 0.1490 | 27.89 |
| nano-NiO | optimized Fisher's FF | | |
| $Ni^{+2}$—$O^{-2}$ | 754.92 | 0.3310 | 0.0 |
| $O^{-2}$—$O^{-2}$ | 22764.3 | 0.1505 | 27.89 |

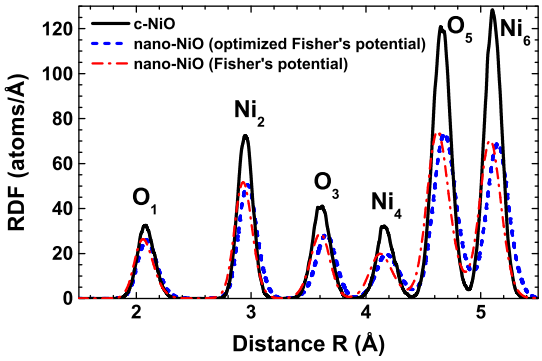


**Fig. 4.** The total radial distribution functions (RDFs) $G(R)$, including Ni—O and Ni—Ni correlations, for c-NiO (solid line) and nano-NiO (dashed lines — optimized Fisher's force field (FF); dash-dot line — Fisher's FF [42]) obtained from molecular dynamics simulations. Note the progressive coordination number reduction for nano-NiO. The first six coordination shells ($O_1$, …, $Ni_6$) are labeled.

The scattering potentials and partial phase shifts were evaluated only once for the average configuration, thus neglecting a variation of the scattering potentials due to thermal vibrations [3]. The multiple-scattering effects were taken into account up to the eights order with the half path length up to 6.5 Å. The inelastic losses were taken into account using the complex exchange-correlation Hedin–Lundqvist potential [3]. The cluster potential, used in the scattering amplitudes calculation, was of muffin-tin (MT) type, and the values of the MT-radii were $R_{MT}(Ni) = 1.319$ Å and $R_{MT}(O) = 1.021$ Å. The configuration-averaged EXAFS signal was obtained by averaging over several thousands configurations (normally 4000), and its convergence was controlled. The calculations were performed using the cluster-type computer at ISSP [44].

## 4. Results

The normalized to the absorption edge jump Ni K-edge XANES signals for crystalline and nanocrystalline nickel oxide are compared in Fig. 1. They are composed of the low energy pre-edge peak A at ~8335 eV, the main maximum at ~8347 eV, and the fine structure above it. The two XANES signals are very close, except that the main maximum and the broad peak at ~8400 eV have slightly higher intensity in c-NiO. The pre-edge region of the XANES provides with the information on the local electronic structure at the absorbing Ni atoms in the presence of the core-hole. In particular, the Ni K-edge absorption is caused by the transition of a 1 s electron of nickel from its core atomic state to a final unoccupied state following to dipole ($\Delta l = \pm 1$) or quadrupole ($\Delta l = 0, \pm 2$) selection rules. Note that the final state is a relaxed excited state due to the presence of a 1 s core hole screened by the other electrons of nickel.

The results of the best-fit analysis of the Ni K-edge EXAFS $\chi(k)k^2$ signals from the first two peaks in FTs (Fig. 2), corresponding mainly to the first two coordination shells around nickel, has been performed in c-NiO and nano-NiO using conventional two-shell approach within the single-scattering approximation [33] as described in Section 2. Only the contributions from the first and second coordination shells, composed of oxygen ($O_1$) and nickel ($Ni_2$) atoms, respectively, were considered and provided good agreement between calculated and experimental EXAFS signals (Fig. 3). The obtained values of the structural parameters ($N$, $R$, $\sigma^2$) are reported in Table 1. Note that the coordination numbers and interatomic distances in bulk c-NiO agree well with the known crystallographic values ($N_{XRD}(O_1) = 6$, $R_{XRD}(Ni-O_1) = 2.089$ Å, and $N_{XRD}(Ni_2) = 12$, $R_{XRD}(Ni-Ni_2) = 2.954$ Å [35].

Next, the total configuration-averaged Ni K-edge EXAFS $\chi(k)k^2$ signals were calculated within the multiple-scattering approximation (Figs. 6 and 7), based on the results of the classical molecular dynamics simulations as described in Section 3. Two sets of the force-field parameters (Table 2), originally found by Fisher [42] and Oliver [43], were used in the case of c-NiO. The comparison between the experimental and calculated EXAFS signals suggests slightly better agreement in the case of the Fisher's FF model, particularly for the second peak in FT at 2.6 Å (Fig. 5): therefore, it was used in the further analysis. Note that to reproduce the atomic structure relaxation in nano-NiO, the potential parameters $\rho$ of the original Fisher's FF model were optimized for both Ni—O and O—O interactions (Table 2), till the good agreement between the experimental and calculated EXAFS signals for nanocrystalline oxide was achieved (Fig. 7).

The importance of the high-order atomic correlations, contributing into the total EXAFS signal through the multiple-scattering events, is evidenced in Figs. 6 and 7. Here, the contributions into the total EXAFS signal from the single-scattering (SS) and multiple-scattering (MS) (up to the sixth order) events are compared in $k$- and $R$-space. In both c-NiO and nano-NiO, the MS effects are important at all $k$-values, being responsible for nearly half or more of the EXAFS oscillations amplitude starting from $k \approx 3.5$ Å$^{-1}$. In $R$-space, the MS contribution is absent under the first two peaks ($R \leq 3$ Å), but becomes comparable to or even dominating that from the SS events at longer distances.

The total RDFs $G(R)$ for c-NiO and nano-NiO (Fig. 4), including Ni—O and Ni—Ni correlations and obtained during the MD runs, were used to determine a set of structural parameters as coordination numbers $N$, interatomic distances $R$, and MSRDs $\sigma^2$ for the first six coordination shells (Table 3). This was done by the decomposition of $G(R)$ into a set of Gaussian functions. Thus obtained values of $N$ and $R$ for c-NiO are in good agreement with crystallographic data. For nano-NiO, two sets of structural parameters were found, corresponding to the original [42] and optimized Fisher's force fields. The main difference between them is observed only in the values of interatomic distances, being due to different $\rho$ values in the Buckingham potential (Table 2). The coordination numbers $N$ in nano-NiO are reduced compared to c-NiO (Table 3): the effect increases with the interatomic distance due to the surface termination effect, as expected.

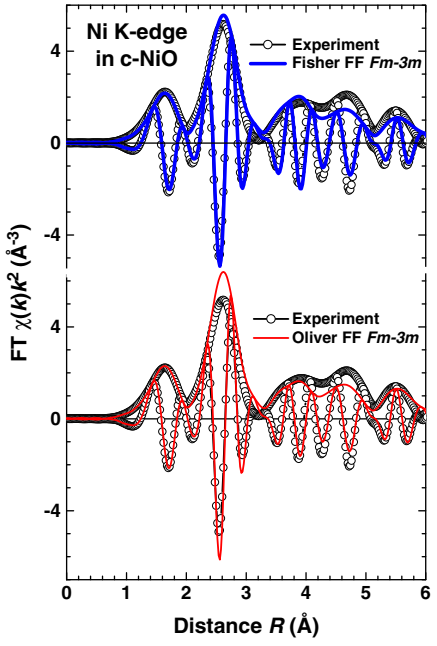


**Fig. 5.** Comparison of experimental (open circles) and calculated (solid lines) Ni K-edge EXAFS $\chi(k)k^2$ signals and their Fourier transforms for c-NiO. The simulations were performed for the cubic $Fm-3m$ c-NiO phase using the Oliver's [43] and Fisher's [42] force fields (FF).

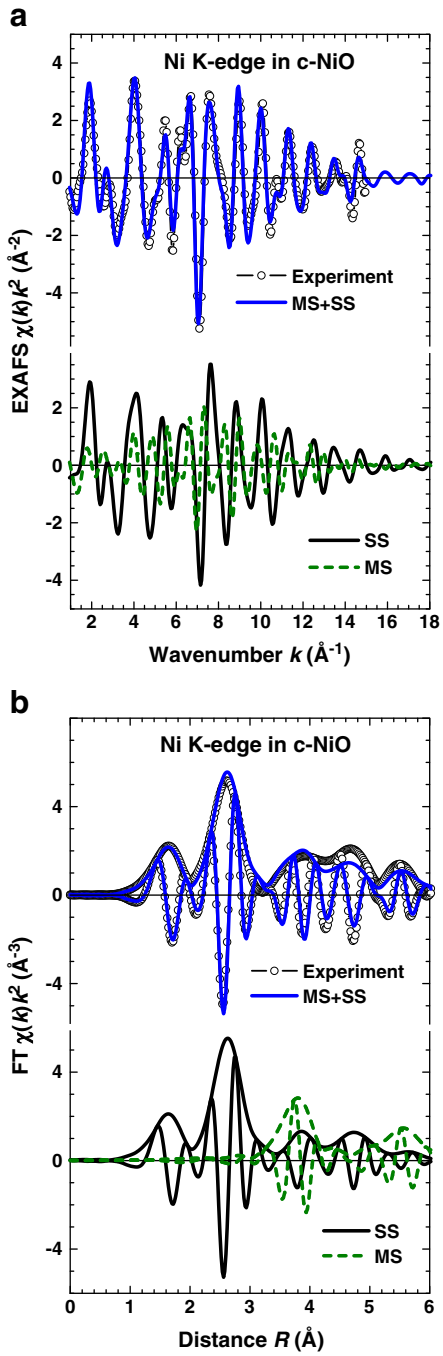


**Fig. 6.** Comparison of experimental (open circles) and total calculated (upper solid line) Ni K-edge EXAFS $\chi(k)k^2$ signals and their Fourier transforms for c-NiO. The two lower curves in both panels correspond to the multiple-scattering (MS) (dashed line) and single-scattering (SS) (lower solid line) contributions into the total calculated EXAFS signal.

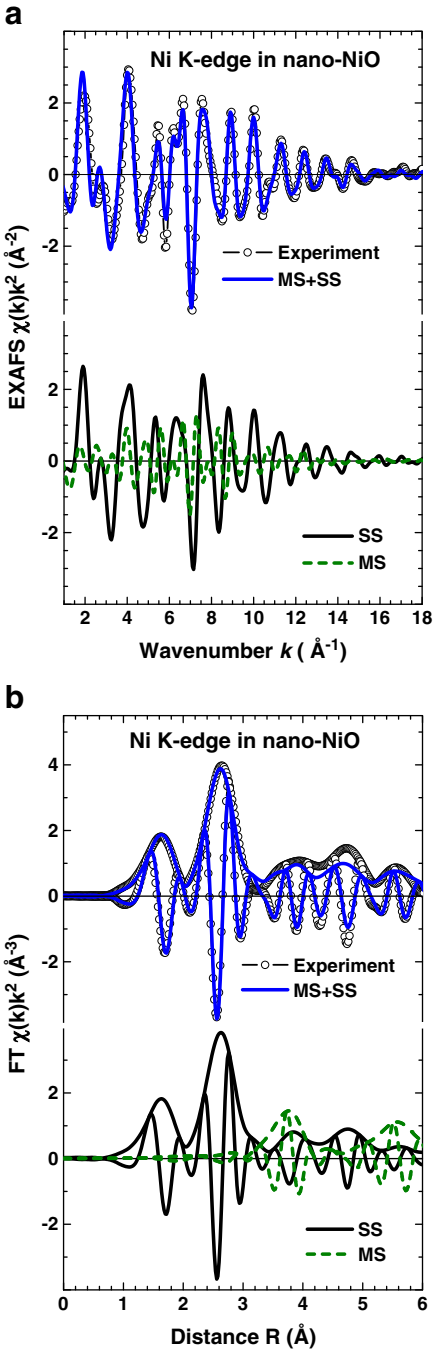


**Fig. 7.** Comparison of experimental (open circles) and total calculated (upper solid line) Ni K-edge EXAFS $\chi(k)k^2$ signals and their Fourier transforms for nano-NiO. The two lower curves in both panels correspond to the multiple-scattering (MS) (dashed line) and single-scattering (SS) (lower solid line) contributions into the total calculated EXAFS signal.

## 5. Discussion

The interpretation of the Ni K-edge XANES in NiO has been a topic of extensive studies in the past [27,45–51]. The use of the multiple-scattering approach allowed understanding the origin of main peaks to be due to the scattering by atoms of the first ten coordination shells surrounding the absorber [45,48]. The pre-edge peak A (Fig. 1) was assigned to the quadrupole 1s → 3d transition from the analysis of resonant x-ray magnetic scattering in [46]. Its quadrupole origin was also supported by several theoretical calculations [47,49,50].

In the recent work [51], the DFT + $U$ calculation scheme, i.e., the density-functional theory (DFT) with the Hubbard-$U$ correction obtained by linear response, within the spin-polarized generalized gradient approximation (GGA) was applied to the analysis of Ni K-edge in NiO. It was found that the pre-edge peak A consists of two contributions: (i) a quadrupole part caused by the intrasite 1s (Ni) → 3d(Ni) excitations lowered by core-hole attraction, and (ii) a very small dipolar component due to the 3d(Ni)-2p(O) hybridization between nearest Ni and O atoms [51]. At the same time, the next feature B of dipolar origin (Fig. 1) has nonlocal nature, caused by hybridization of on-site Ni empty 4p states with empty 3d states of the Ni atoms

**Table 3**
Structural parameters ($N$ is the coordination number, $R$ is the interatomic distance, and $\sigma^2$ is the MSRD) for the first six coordination shells in c-NiO and nano-NiO obtained by decomposition of the Ni—O and Ni—Ni RDFs into Gaussian components.

| | $O_1$ | $Ni_2$ | $O_3$ | $Ni_4$ | $O_5$ | $Ni_6$ |
|---|---|---|---|---|---|---|
| *c-NiO* | | | | | | |
| $N$ | 6 | 12 | 8 | 6 | 24 | 24 |
| $R$ (Å) | 2.083 | 2.949 | 3.610 | 4.167 | 4.661 | 5.106 |
| $\sigma^2$ (Å$^2$) | 0.0055 | 0.0042 | 0.0059 | 0.0056 | 0.0062 | 0.0057 |
| *nano-NiO (optimized Fisher's FF)* | | | | | | |
| $N$ | 5.4 | 10.0 | 6.1 | 5.0 | 18.3 | 16.8 |
| $R$ (Å) | 2.092 | 2.970 | 3.647 | 4.185 | 4.688 | 5.147 |
| $\sigma^2$ (Å$^2$) | 0.0071 | 0.0063 | 0.0075 | 0.0104 | 0.0101 | 0.0097 |
| *nano-NiO (Fisher's FF [42])* | | | | | | |
| $N$ | 5.4 | 10.0 | 6.1 | 5.0 | 18.3 | 16.8 |
| $R$ (Å) | 2.066 | 2.933 | 3.601 | 4.132 | 4.629 | 5.082 |
| $\sigma^2$ (Å$^2$) | 0.0069 | 0.0060 | 0.0072 | 0.0101 | 0.0099 | 0.0093 |
| $N_{nano}/N_{cryst}$ | 0.90 | 0.83 | 0.76 | 0.83 | 0.76 | 0.70 |

located in the fourth coordination shell [51] and participating in the 180° Ni—O—Ni antiferromagnetic interactions. Due to the nonlocal origin of the feature B, its position is insensitive to the core-hole attraction and, thus, the A-to-B peak separation can be used to estimate the value of the charge transfer gap in NiO [51]. The similarity of the XANES signals in bulk c-NiO and nano-NiO (Fig. 1) suggests the closeness of their electronic structures: in particular, one can conclude that no significant changes in the spin ordering should occur in NiO upon a decrease of the crystallites size down to ~6 nm.

The difference between the Ni K-edge EXAFS signals of c-NiO and nano-NiO is much more pronounced than between their XANES signals: it appears mainly in the amplitude damping and a difference in the frequency of oscillations — both effects are better observed at high $k$-values (Fig. 2). The Fourier transforms (FTs) of the EXAFS signals demonstrate the progressive lowering of the peaks amplitude at larger $R$-values. Such behavior is related to the nanosized effect [27,52], which includes both the reduction of coordination number due to an increase of the number of under-coordinated atoms at the nanocrystals surface and an increase of the disorder due to the nanoparticles structure relaxation.

In nano-NiO three effects can be observed: (i) the average coordination numbers $N$ decrease due to the under-coordinated atoms located at the nanocrystals surface; (ii) the interatomic distances behave differently in the first and the second shells — the Ni—$O_1$ distance decreases by ~0.01 Å, whereas the Ni–$Ni_2$ increases by about the same amount; (iii) the MSRD values in both shells have larger values than in bulk c-NiO. Thus, one can conclude that the local structure in nano-NiO relaxes leading to an increase of disorder.

Detailed comparison of the total EXAFS signals in Fig. 2 allows one to notice that the phase difference of the EXAFS oscillations increases progressively from low to high wavenumber values in nano-NiO compared to c-NiO. This fact reflects the difference in the average lattice parameters ($a_0$) in two samples. Their values, estimated from Ni—$Ni_2$ distances, are equal to $a_0 = 4.188$ Å for nano-NiO and $a_0 = 4.171$ Å for c-NiO. The latter value agrees well with the x-ray diffraction results $a_0 = 4.1773$ Å for c-NiO [35]. Assuming the cubic shape for nanoparticles, one can evaluate the change in the lattice volume being $\Delta V/V_0 \simeq 1\%$ ($V_0 = 72.5$ Å$^3$ for c-NiO and $V = 73.43$ Å$^3$ for nano-NiO). Thus, our data confirm the expansion of the nano-NiO lattice, found recently by x-ray diffraction [25,26].

Further we will discuss the contributions from the outer shells (beyond the second one) into the total EXAFS signal. Their reliable analysis is a challenge, that requires correct account for the multiple-scattering (MS) effects. The peculiarity of the NiO crystal structure is responsible for the presence of many linear MS paths with large relative amplitude. Therefore, to address this problem, we used recently developed approach [3], allowing the calculation of the configuration-averaged EXAFS signal based on the results of the MD simulations.

First, we will discuss the results for bulk c-NiO. The MD simulations were performed using two FF potential models, developed in the past by Fisher [42] and Oliver [43]. The two models include the same pair interactions, but differ slightly in the numerical values of the FF parameters (Table 2).

In Fig. 5 the configuration-averaged EXAFS signals, calculated using two FF models, are compared with the experiment for c-NiO. The observed agreement is good, especially taking into account the simplicity of the models. Note that no fitting parameters were used in the calculations. More detailed comparison of the two models suggested that the Fisher's FF model [42] provides slightly better agreement in the FT region of the second peak at ~2.6 Å: therefore, only it will be considered further.

The detailed contributions from single-scattering (SS) and multiple-scattering (MS) processes in c-NiO and nano-NiO are shown in Figs. 6 and 7. As one can see, the MS signals are inevitably important in both materials in the region of the third peak at 3.8 Å and of the fifth peak at 5.6 Å. Note that all signals in Figs. 6 and 7 entirely contain thermal disorder effects. Besides, the EXAFS signal for nano-NiO, calculated for a particle size of $6a_0 \times 6a_0 \times 6a_0$, takes into account both lattice expansion and surface termination effects. The agreement between calculated and experimental EXAFS signals in nano-NiO is good, however our simple FF model is not able to reproduce the relaxation of the first coordination shell in nano-NiO, found by the conventional analysis (Table 2). Our preliminary estimate indicates that this phenomenon may be due to the presence of Ni vacancies in nano-NiO and will be the subject of subsequent work.

The atomic structure of c-NiO and nano-NiO can be conveniently described in terms of the radial distribution functions. The total RDFs $G(R)$, obtained from a set of atomic configurations collected during the MD runs, are reported in Fig. 4 for the first six coordination shells of nickel atoms. The shape of the peaks in the RDFs can be sufficiently well approximated by the Gaussian function that allows one to separate shells contributions and to obtain for each shell the values of structural parameters as coordination numbers $N$, interatomic distances $R$, and MSRDs $\sigma^2$. Their variation on going from c-NiO to nano-NiO with the optimized Fisher's force-field is well seen in Table 3.

In particular, the coordination numbers $N$ in nano-NiO are reduced compared to c-NiO, and the effect increases, as expected, with the interatomic distance due to the surface termination effect. The coordination shells radii, i.e. interatomic distances $R$, increase in nano-NiO due to the change in the FF potential model (Table 2), required to reproduce the lattice expansion. The significant difference is also observed between the MSRD values in nano-NiO and c-NiO. In the bulk, the MSRD describes the thermal disorder contribution. The thermal atoms motion is partially correlated for the nearest atoms, due to the direct chemical bonding. However, when the correlation effects in thermal motion at large distances become negligible, the MSRD value approaches towards a sum of the mean-squared displacements (MSD) for the two atoms. Therefore, the MSRD for the atom pair A and B is given by

$$\mathrm{MSRD_{AB}} = \mathrm{MSD_A} + \mathrm{MSD_B} - \mathrm{DCF_{AB}} \quad (2)$$

where DCF is the displacement correlation function [53].

The MSD values can be experimentally determined from diffraction measurements: MSD(O) = 0.0032 Å$^2$ and MSD(Ni) = 0.0028 Å$^2$ for c-NiO at 300 K [41]. This means that the values of the MSRDs equal to 0.0060 Å$^2$ and 0.0056 Å$^2$ are expected for Ni—O and Ni—Ni atom pairs, respectively, for uncorrelated motion (DCF = 0) at large distances. Note that these values are in good agreement with our simulation results for the fifth and sixth coordination shells (Table 3).

In nano-NiO, the softening of interaction potentials leads to the lattice expansion and to an increase of the amplitude of thermal

vibrations (see optimized Fisher's FF model in Table 3). Besides, the distribution of structural sites contributes additionally to an increase of the MSRDs since atoms located closer to the nanoparticle surface have vibration amplitude larger than the ones being closer to the nanoparticle center. Therefore, the average MSRDs are larger by about 0.002–0.004 Å$^2$ in nano-NiO compared to c-NiO (Table 3).

The results obtained in the present work are also relevant to other compounds incorporating NiO nanocrystals or fragments of NiO structure. For example, the formation of NiO nanoclusters and nanodomains was found in alkali borate glasses containing 0.5–2.0 wt.% of nickel oxide [54,55]. It was observed that the size of Ni-enriched nanodomains depends on the glass composition and decreases as the alkali content increases [55], indicating strong interaction between nanodomains and glass matrix. The size reduction of NiO nanodomains in the glasses is also accompanied by a decrease of the first coordination shell Ni—O distance [55], similar to our findings in nanoparticles (Table 1). However, the Ni—O distance variation in the glasses is much stronger and was attributed to the decrease of the nickel coordination number from six (for $R$(Ni—O) = 2.05–2.07 Å) to four (for $R$(Ni—O) = 1.95–1.98 Å) oxygen atoms [55].

## 6. Conclusions

The local structure and its relaxation around nickel atoms were studied in nanocrystalline nickel oxide (nano-NiO) by the Ni K-edge x-ray absorption spectroscopy.

Using conventional multi-shell single-scattering approach to the analysis of the first two coordination shells around nickel, we found that the lattice in nano-NiO expands compared to bulk nickel oxide (c-NiO), in agreement with other studies by EXAFS [27,52] and XRD [25,26]. The change in the lattice parameter (Table 1) corresponds to the volume expansion in nano-NiO by about 1%. At the same time, a contraction of the Ni—O bond by about 0.5% was observed in the first coordination shell in nano-NiO. Note that similar effect has been previously detected in NiO thin films [27,52].

The EXAFS signals generated within the first six coordination shells around nickel atoms (cluster size up to ~6.5 Å) were next analyzed in bulk c-NiO and nano-NiO by the approach [3], based on a combination of classical molecular dynamics (MD) and ab initio multiple-scattering EXAFS theory. The classical MD simulations of c-NiO were performed for the two force-field (FF) models originally developed by Fisher [42] and Oliver [43] (Fig. 5 and Table 2). The results obtained with the Fisher's FF model provided better agreement between configuration-averaged and experimental Ni K-edge EXAFS signals; therefore it was used further for the simulation of nano-NiO.

In nanosized NiO, we found that original Fisher's FF model fails to reproduce the lattice expansion and total EXAFS signal (Fig. 6). However, the model can be corrected by adjusting the $\rho$ parameter of the Buckingham potentials (Table 2) to make them more repulsive.

To conclude, we showed that the MD-EXAFS simulations of the Ni K-edge in c-NiO and nano-NiO, based on simple rigid-ion force-field model, provide rather good agreement with the experiment. Such approach requires less parameters than conventional EXAFS analysis and allows accounting explicitly for thermal effects and many-atom distribution functions. The agreement between the experimental and calculated EXAFS signals can be used as a criterion to optimize the parameters of the force-field models, thus opening a new possibility for accurate potential model development.

## Acknowledgments

This work was supported by ESF Project 2009/0202/1DP/1.1.1.2.0/09/APIA/VIAA/141 and Latvian Government Research Grant No. 09.1518. The research leading to these results has received funding from the European Community's Seventh Framework Programme (FP7/2007-2013) under grant agreement No. 226716 (Projects I-20090071 EC and I-20100110 EC).

## References

[1] S.J.L. Billinge, I. Levin, Science 316 (2007) 561.
[2] S.J.L. Billinge, J. Solid State Chem. 181 (2008) 1695.
[3] J.J. Rehr, R.C. Albers, Rev. Mod. Phys. 72 (2000) 621.
[4] M. Benfatto, C.R. Natoli, A. Filipponi, Phys. Rev. B 40 (1989) 9626.
[5] A. Filipponi, A. Di Cicco, C.R. Natoli, Phys. Rev. B 52 (1995) 15122.
[6] A. Filipponi, A. Di Cicco, Phys. Rev. B 52 (1995) 15135.
[7] P. Kizler, Phys. Rev. B 67 (1991) 3555.
[8] B.J. Palmer, D.M. Pfund, J.L. Fulton, J. Phys. Chem. B 100 (1996) 13393.
[9] P. D'Angelo, A. Di Nola, M. Mangoni, N.V. Pavel, J. Chem. Phys. 104 (1996) 1779.
[10] P.J. Merkling, A. Muñoz-Páez, R.R. Pappalardo, M.E. Sánchez, Phys. Rev. B 64 (2001) 092201.
[11] D. Cabaret, M. Le Grand, A. Ramos, A.M. Flank, S. Rossano, L. Galoisy, G. Calas, D. Ghaleb, J. Non-Cryst. Solids 289 (2001) 1.
[12] Y. Okamoto, Nucl. Instrum. Meth. Phys. Res. A 526 (2004) 572.
[13] F. Farges, Y. Lefrère, S. Rossano, A. Berthereau, G. Calas, G.E. Brown Jr., J. Non-Cryst. Solids 344 (2004) 176.
[14] A. Di Cicco, A. Trapananti, J. Phys. Condens. Matter 17 (2005) S135.
[15] G. Ferlat, J.C. Soetens, A. SanMiguel, P.A. Bopp, J. Phys. Condens. Matter 17 (2005) S145.
[16] S.J. Gurman, R.L. McGreevy, J. Phys. Condens. Matter 2 (1990) 9463.
[17] M. Winterer, J. Appl. Phys. 88 (2000) 5635.
[18] R.L. McGreevy, J. Phys. Condens. Matter 13 (2001) R877.
[19] C.Q. Sun, Prog. Solid State Chem. 35 (2007) 1.
[20] S. Tsunekawa, K. Ishikawa, Z.-Q. Li, Y. Kawazoe, A. Kasuya, Phys. Rev. Lett. 85 (2000) 3440.
[21] M. Fukuhara, Phys. Lett. A 313 (2003) 427.
[22] G. Li, J. Boerio-Goates, B.F. Woodfield, L. Li, Appl. Phys. Lett. 85 (2004) 2059.
[23] A. Kossoy, Y. Feldman, E. Wachtel, K. Gartsman, I. Lubomirsky, J. Fleig, J. Maier, Phys. Chem. Chem. Phys. 8 (2006) 1111.
[24] R.N. Bhowmik, R. Ranganathan, R. Nagarajan, Phys. Rev. B 73 (2006) 144413.
[25] L. Li, L. Chen, R. Qihe, G. Li, Appl. Phys. Lett. 89 (2006) 134102.
[26] M. Ghosh, K. Biswas, A. Sundaresana, C.N.R. Rao, J. Mater. Chem. 16 (2006) 106.
[27] A. Kuzmin, J. Purans, A. Rodionov, J. Phys. Condens. Matter 9 (1997) 6979.
[28] A. Corrias, G. Mountjoy, G. Piccaluga, S. Solinas, J. Phys. Chem. B 103 (1999) 10081.
[29] E. Groppo, C. Prestipino, C. Lamberti, P. Luches, C. Giovanardi, F. Boscherini, J. Phys. Chem. B 107 (2003) 4597.
[30] A. Kuzmin, J. Purans, J. Phys. Condens. Matter 5 (1993) 9423.
[31] A. Kuzmin, R.A. Evarestov, J. Phys. Condens. Matter 21 (2009) 055401.
[32] A. Kuzmin, Phys. B 208 (209) (1995) 175.
[33] V.L. Aksenov, M.V. Kovalchuk, A.Yu. Kuzmin, Yu. Purans, S.I. Tyutyunnikov, Cryst. Rep. 51 (2006) 908.
[34] A.L. Ankudinov, B. Ravel, J.J. Rehr, S.D. Conradson, Phys. Rev. B 58 (1998) 7565.
[35] A. Kuzmin, N. Mironova, J. Phys. Condens. Matter 10 (1998) 7937.
[36] A. Kuzmin, R.A. Evarestov, J. Phys. Conf. Ser. 190 (2009) 012024.
[37] S. Brunauer, P.H. Emmett, E. Teller, J. Am. Chem. Soc. 60 (1938) 309.
[38] A. Kalinko, R.A. Evarestov, A. Kuzmin, J. Purans, J. Phys. Conf. Ser. 190 (2009) 012080.
[39] J.D. Gale, A.L. Rohl, Mol. Simul. 9 (2003) 291.
[40] W.L. Roth, Phys. Rev. 110 (1958) 1333.
[41] D. Rodic, V. Spasojevic, V. Kusigerski, R. Tellgren, H. Rundlof, Phys. Status Solidi B 218 (2000) 527.
[42] C.A.J. Fisher, Scr. Mater. 50 (2004) 1045.
[43] P.M. Oliver, G.W. Watson, S.C. Parker, Phys. Rev. B 52 (1995) 5323.
[44] A. Kuzmin, Latv. J. Phys. Tech. Sci. 2 (2006) 7.
[45] P. Kizler, Phys. Rev. B 46 (1992) 10540.
[46] J.P. Hill, C.-C. Kao, D.F. McMorrow, Phys. Rev. B 55 (1997) R8662.
[47] R.V. Vedrinskii, V.L. Kraizman, A.A. Novakovich, Sh.M. Elyafi, S. Bocharov, Th. Kirchner, G. Dräger, Phys. Status Solidi B 226 (2001) 203.
[48] H. Modrow, S. Bucher, J.J. Rehr, A.L. Ankudinov, Phys. Rev. B 67 (2003) 035123.
[49] Z.Y. Wu, D.C. Xian, T.D. Hu, Y.N. Xie, Y. Tao, C.R. Natoli, E. Paris, A. Marcelli, Phys. Rev. B 70 (2004) 033104.
[50] A. Kuzmin, J. Purans, R. Kalendarev, Phys. Status Solidi C 2 (2005) 665.
[51] C. Gougoussis, M. Calandra, A. Seitsonen, Ch. Brouder, A. Shukla, F. Mauri, Phys. Rev. B 79 (2009) 045118.
[52] E. Avendano, A. Kuzmin, J. Purans, A. Azens, G.A. Niklasson, C.G. Granqvist, Phys. Scr. T115 (2005) 464.
[53] G. Beni, P.M. Platzman, Phys. Rev. B 14 (1976) 1514.
[54] L. Galoisy, G. Calas, L. Cormier, J. Non-Cryst. Solids 293 (2001) 105.
[55] L. Galoisy, G. Calas, L. Cormier, J. Non-Cryst. Solids 321 (2003) 197.